nanomaterials

MDPI

Article

Preparation of TiO_2/Carbon Nanotubes/Reduced Graphene Oxide Composites with Enhanced Photocatalytic Activity for the Degradation of Rhodamine B

Yanzhen Huang [1], Dongping Chen [2], Xinling Hu [2], Yingjiang Qian [2] and Dongxu Li [1,2,*]

[1] College of Materials Science and Engineering, Huaqiao University, Xiamen 361021, China; 1611302044@hqu.edu.cn

[2] Fujian Key Laboratory of Photoelectric Functional Materials, Huaqiao University, Xiamen 361021, China; 1511302044@hqu.edu.cn (D.C.); 1611302043@hqu.edu.cn (X.H.); 17013081050@hqu.edu.cn (Y.Q.)

* Correspondence: lidongxu@hqu.edu.cn; Tel.: +86-592-616-2225

Received: 17 May 2018; Accepted: 11 June 2018; Published: 13 June 2018

Abstract: In this report, ternary titanium dioxide (TiO_2)/carbon nanotubes (CNTs)/reduced graphene oxide (rGO) composites were fabricated by a facile and environmentally friendly one-pot solvethermal method for the removal of Rhodamine B (RhB). Its structures were represented by X-ray powder diffraction (XRD), Raman spectrometry, scanning electron microscopy (SEM) and transmission electron microscopy (TEM). The photocatalytic performance was tested by the degradation efficiency of RhB under UV-vis light irradiation. The experimental results indicated that photocatalytic activity improved as the ratio of CNTs:TiO_2 ranged from 0.5% to 3% but reduced when the content increased to 5% and 10%, and the TiO_2/CNTs/rGO-3% composites showed superior photocatalytic activity compared with the binary ones (i.e., TiO_2/CNTs, TiO_2/rGO) and pristine TiO_2. The rate constant k of the pseudo first-order reaction was about 1.5 times that of TiO_2. The improved photocatalytic activity can be attributed to the addition of rGO and CNTs, which reduced the recombination of photo-induced electron-hole pairs, and the fact that CNTs and rGO, with a high specific surface area and high adsorption ability to efficiently adsorb O_2, H_2O and organics, can increase the hydroxyl content of the photocatalyst surface.

Keywords: titanium dioxide; carbon nanotubes; graphene; photocatalyst

1. Introduction

Photocatalysts have aroused extensive interest for their effective treatment of organic contaminations which were degraded into small molecules of carbon dioxide (CO_2) and water [1,2]. Anatase titanium dioxide (TiO_2), with a 3.2 eV band gap, has been extensively researched as a photocatalyst because of its high photocatalytic activity, high stability, low toxicity and low cost [3–5]. However, as we all know, electron-hole recombination and the low availability of sunlight have been disadvantages that have reduced the photocatalytic activity [6,7]. Plentiful research works, such as those on noble metal deposition [8,9], transition metal or non-metallic elements dopants [10,11], metal oxide deposition [12,13] and preparation of carbon-based TiO_2 compounds [14–16], have been done to solve the aforementioned problems.

Graphene has received wide study due to its distinct properties such as its outstanding charge-carrier mobility (~250,000 $cm^2 \cdot V^{-1} \cdot s^{-1}$ at room temperature), high thermal conductivity (~5000 $W \cdot m^{-1} \cdot K^{-1}$), high mechanical stiffness (~1 TPa) and high specific surface area (~2600 $m^2 \cdot g^{-1}$) for the preparation of photocatalyst composites [17,18]. Therefore, graphene can be applied

to synthesize photocatalysts to increase the electron-hole separation efficiency and enhance the photocatalytic activity. Singh et al. [19] reported the photodegradation rate of water-soluble graphene nanosheets (wsGNS) isolated from toxic black pollutants was almost 11 times that of insoluble graphene nanosheets (GNS) to methyl blue (MB) under visible light. Zhang et al. [20] applied TiO_2/graphene composites to degrade methyl orange (MO) and found that the photocatalytic activity of TiO_2/graphene was higher than that of P25 and graphene. Pan et al. [7] incorporated graphene into TiO_2 nanowires and obtained a preferable property for the removal of MB compared to TiO_2 nanowires. Shiraishi et al. [21] reported that TiO_2/reduced graphene oxide compounds yielded cyclohexanone with twice the amount formed on bare TiO_2. Owing to the high surface to volume ratio, nanoscale ZnO particles have become rather vital to synthesize compounds [22]. Malekshoar et al. [23] proved a 30% improvement on the degradation rate of phenol by ZnO-graphene compared with ZnO. Fu [24] prepared a ZnO/TiO_2 coupled film and researched the photocatalytic degradation activity of RhB. Carbon quantum dots, a kind of zero-dimensional nanomaterials, have received much attention due to their optical, physical and chemical properties. Tyagi et al. [25] detected the catalytic performance of TiO_2-water soluble carbon quantum dots (wsCQDs) was ~1.5 times more than that of TiO_2. Gogoi et al. [26] applied polymer-supported carbon dots to produce hydrogen peroxide. Another latent carbon material, carbon nanotubes (CNTs), are a kind of one-dimensional nanomaterial with high surface area and excellent conductivity [27]. Xiong et al. [28] proved that Fe/N-CNTs demonstrated better photocatalytic activity compared with Fe/CNTs to CO conversion. Jiang et al. [29] demonstrated that, when the doped graphitic-like N content was 6.22 at.%, nitrogen-doped carbon nanotube (NCNT)-supported NiO (NiO/NCNTs) showed the best photocatalytic oxidation property to toluene. Zhang et al. [30] disclosed that Pt/N-multiwalled CNTs (MWCNTs) possessed a higher selective oxidation of glycerol compared with Pt/MWCNTs. Liu et al. [31] developed a one-pot chemical method to synthesize anatase TiO_2 onto MWCNTs which showed higher activity for the photocatalytic degradation of MO compared to pristine TiO_2. Tetty et al. [32] demonstrated the reaction rate of MWCNTs/TiO_2 fabricated through layer-by-layer assembly was one time higher than that of TiO_2 to degrade Procion Red MX-50 (PR). Yen et al. [33] prepared a MWCNTs/TiO_2 hybrid which displayed better photocatalytic activity for nitric oxide (NO) oxidation. With the development of carbon materials, many scientists have applied themselves to unite CNTs/rGO with metal oxide to receive ternary composites with an out-bound property. The CNTs loaded on rGO sheets would serve as charge transfer channels, which might strengthen the electrical property of rGO. Moreover, CNTs could prevent the stacking of rGO sheets and provide a larger surface area which would be beneficial to the photocatalytic performance.

Herein, TiO_2 have been deposited on CNTs/rGO by a simple one-pot method. The effect that the mass ratio of CNTs to TiO_2 has on photocatalytic properties was explored, and an optimum ratio was obtained. Furthermore, the as-prepared TiO_2/CNTs/rGO-3% composites showed superior photocatalytic activity compared with the binary ones (i.e., TiO_2/CNTs, TiO_2/rGO) and pristine TiO_2.

2. Experimental Part

2.1. Sample Preparation

Graphene oxide (GO, with diameter of 10~25 μm, thickness of 0.8~1.2 nm) was purchased from Shanghai Jiuai Biotechnology Co., Ltd. (Shanghai, China). CNTs (with diameter 60~100 nm, length > 5 μm) were purchased from Shenzhen Nanotech Port Co., Ltd. (Shenzhen, China).

TiO_2/CNTs/rGO composites were synthesized by the solvethermal method. The CNTs were dissolved in 75 mL nitric acid (65%~68%), sonicated for 30 min and placed in a flask which was placed in a thermostatic water bath at 75 °C for 5~8 h. Then, the material was filtered, rinsed and dried at 80 °C overnight. The amount of 30 mg GO and a certain number of oxide-treated CNTs were dispersed in 25 mL of isopropyl alcohol and treated with an ultrasonic processor for 2 h. Then, tetrabutyl titanate (TBT, $C_{16}H_{36}O_4Ti$) was mixed into the above suspension and stirred. This was followed by

adding 1 mL distilled water by dropping. The mixture was transferred to the kettle and heated at 180 °C. The product was filtered, washed with distilled water until PH 7 was reached and dried at 60 °C overnight under vacuum. The quality ratio of CNTs:TiO_2 was 0.5%, 1%, 2%, 3%, 5% and 10%, which were marked as TiO_2/CNTs/rGO-*x*% (*x* = 0.5, 1, 2, 3, 5, 10). The schematic illustration of the TiO_2/CNTs/rGO compound is shown in Figure 1. GO and oxide-treated CNTs were combined through π-π interaction by ultrasonification in homogeneous solution. The SEM images of GO, oxide-treated CNTs, CNTs/GO, TiO_2/CNTs/rGO-3% were displayed in Figure S1. Wang et al. [6] also proved that the photocatalytic performance of TiO_2/CNTs/graphene can be altered by diverse weight ratio of CNTs:TiO_2. For further comparison, the pristine TiO_2, TiO_2/CNTs and TiO_2/rGO were synthesized in accordance with the preparation process of TiO_2/CNTs/rGO-3%.

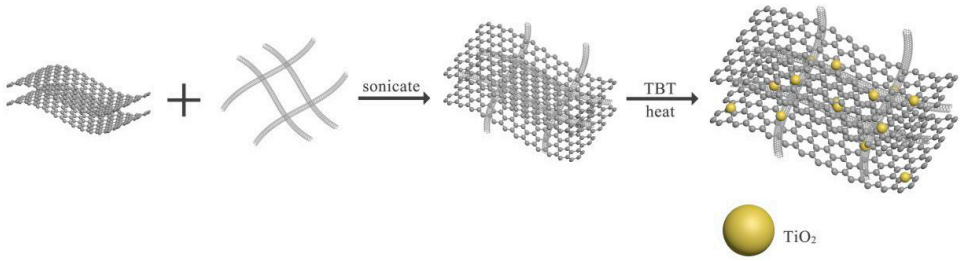

Figure 1. The schematic illustration of TiO_2/carbon nanotubes (CNTs)/ reduced graphene oxide (rGO) composites.

2.2. Characterization

The crystalline phases were characterized by X-ray diffraction (XRD, Rigaku Miniflex 600, Rigaku, Tokyo, Japan) with Cu Kα radiation. Raman spectra were investigated by a micro-Raman spectroscopy system (Raman, inViainVi, London, UK). The surface morphology was obtained by field emission scanning electron microscopy (FESEM, Hitachi, Tokyo, Japan) and transmission electron microscopy (TEM, TECANI F30, FEI, Hillsboro, Nasdaq, USA). Degradation efficiency of RhB was acquired by UV-vis spectrophotometer (Shimadzu UV-2450, Tokyo, Japan).

2.3. Photocatalytic Activity

The experiments of removal of RhB for all photocatalyst composites were conducted under UV-vis light irradiation by a 300 W Xenon lamp (PLS-SXE300UV, Beijing, China) to research the photocatalytic activity. 10 mg of composites were added into a 60 mL 10 mg·L^{-1} RhB solution, sonicated for 10 min and then stirred in the dark for 30 min to guarantee the establishment of an adsorption/desorption equilibrium. During the reaction, 4 mL of solution was taken out every 10 min, centrifuged to remove catalyst particles and finally the degradation efficiency was analyzed with UV-vis spectrophotometer.

3. Results and Discussion

Figure 2a shows the XRD images of TiO_2, TiO_2/rGO, TiO_2/CNTs and TiO_2/CNTs/rGO-3%. The XRD patterns of other composites were shown in Figure S2a. It can be summarized precisely that all diffraction peaks are similar to those of anatase TiO_2 (JCPDF No. 21-1272) [6]. The 2θ peaks appeared at 25.3°, 37.8°, 48.1°, 54.0°, 55.1°, 62.5°, 68.7°, 70.2°, and 75.2° corresponding to (101), (004), (200), (105), (211), (204), (116), (220), and (215) of TiO_2. The fact that no diffraction peak of GO was observed demonstrated that GO might be reduced to rGO (in Figure S3) in the solvethermal process. In addition, the diffraction peak of rGO or CNTs at ~26° was possibly stacked with the leading peak of TiO_2, which was reported in other literature [6,7].

Raman spectroscopy was carried out to analyze the crystal structure of TiO_2 in the composites shown in Figure 2b. The Raman spectra of other composites are presented in Figure S2b. The Raman

patterns of TiO_2/rGO, TiO_2/CNTs, TiO_2/CNTs/rGO-3% showed the characteristic peaks of carbon materials with the presence of D band at 1355 cm^{-1} and G band at 1587 cm^{-1} which were ascribed to sp^3 defects and the in-plane vibration of sp^2 carbon atoms, respectively. The typical peaks at 144 (E_g), 401 (B_{1g}), 520 (B_{1g} + A_{1g}) and 639 cm^{-1} (E_g) of anatase TiO_2 were consistent with the XRD patterns, further inferring the co-existence of TiO_2, rGO and CNTs. The proportions of peak intensities of D and G for TiO_2/rGO, TiO_2/CNTs, TiO_2/CNTs/rGO-3% have been calculated to be 0.98, 0.87 and 1.01, respectively. It is obvious that the I_D/I_G ratio of TiO_2/CNTs/rGO-3% composites was highest, which indicated that TiO_2/CNTs/rGO-3% might be a characteristic of higher level disorder structures and more active sites [34] to improve photocatalytic properties.

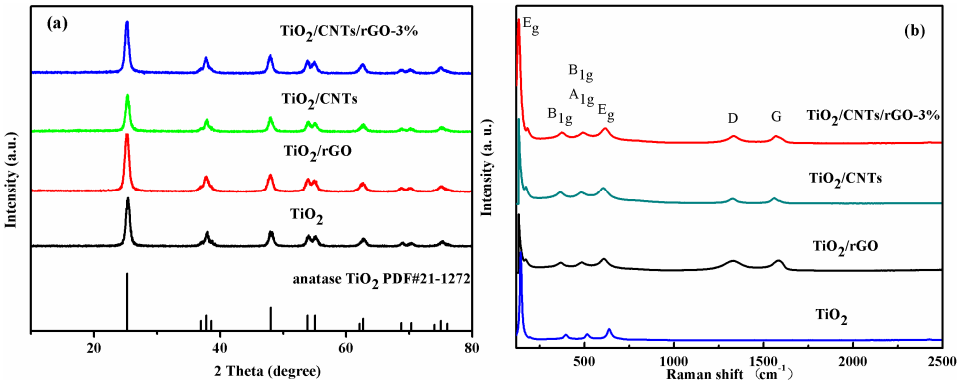

Figure 2. X-ray powder diffraction (**a**) (XRD) patterns; (**b**) Raman spectra of TiO_2, TiO_2/rGO, TiO_2/CNTs and TiO_2/CNTs/rGO-3%.

To further demonstrate the surface topography, the SEM images of TiO_2/rGO and TiO_2/CNTs are shown in Figure 3a,b. TiO_2 nanoparticles were uniformly loaded on two-dimensional rGO sheets with wrinkles which offered a larger surface area, contributing to electron transfer [35], as shown in Figure 3a. We can see that the CNTs substrates were covered by abundant TiO_2 and there were bare CNTs. To further analyze the dispersion state of the ternary composites and particle size of TiO_2, TEM was employed as shown in Figure 3c,d. The high-resolution transmission electron microscopy (HR-TEM) of anatase TiO_2 demonstrated the lattice distance marked in the image was 0.34 nm, corresponding to the XRD results. What is more, the size of TiO_2 was about 10 nm. TiO_2 nanoparticles were not only loaded on rGO sheets but also absorbed on the surface of CNTs, as shown in Figure 3d, and CNTs were intercalated into rGO sheets, which could prevent the stacking of rGO, speed electron migration and improve photocatalytic performance [36].

The photoactivity TiO_2/CNTs/rGO-x% (x = 0.5, 1, 2, 3, 5, 10) was evaluated by degradation of RhB (Figure S4), which showed time profiles of C/C_0 under UV-vis light irradiation, where C is the concentration of RhB at irradiation time t and C_0 the concentration at adsorption/desorption equilibrium before irradiation. The results indicated that photocatalytic activity improved as the ratio of CNTs:TiO_2 ranged from 0.5% to 3%, but it reduced when the content increased, because the carrier transfer and separation were connected with suitable mass ratio and band gap [24]. In order to analyze TiO_2/CNTs/rGO-3% composites in depth, the performance of blank test (RhB photocatalysis alone), TiO_2, TiO_2/rGO and TiO_2/CNTs are represented in Figure 4a. We can clearly see that the activity order from high to low is TiO_2/CNTs/rGO-3% > TiO_2/rGO > TiO_2/CNTs > TiO_2 > blank test. As shown in Figure 4b, the rate constants k were 0.00689, 0.06099, 0.07631, 0.07809 and 0.08785 min^{-1} for blank test, TiO_2, TiO_2/CNTs, TiO_2/rGO, and TiO_2/CNTs/rGO-3%, respectively. After 30 min under UV-vis light, the RhB solution became colorless for TiO_2/CNTs/rGO-3% (Figure S5). TiO_2/CNTs/rGO-3% composites exhibited the best photoactivity whose k was almost 1.5 times that of TiO_2. There are three reasons for this: rGO and CNTs with large surface areas and strong adsorption ability can adsorb O_2, H_2O and organics to increase the content of OH· and improve photocatalytic

activity [37,38]; CNTs improved the oxidation-reduction ability and decreased the recombination efficiency of photo-inducd electron-hole pairs [39]; and CNTs prevented the stacking of rGO and enlarged the distance of rGO sheets that can enrich the active sites for photocatalytic reaction [40].

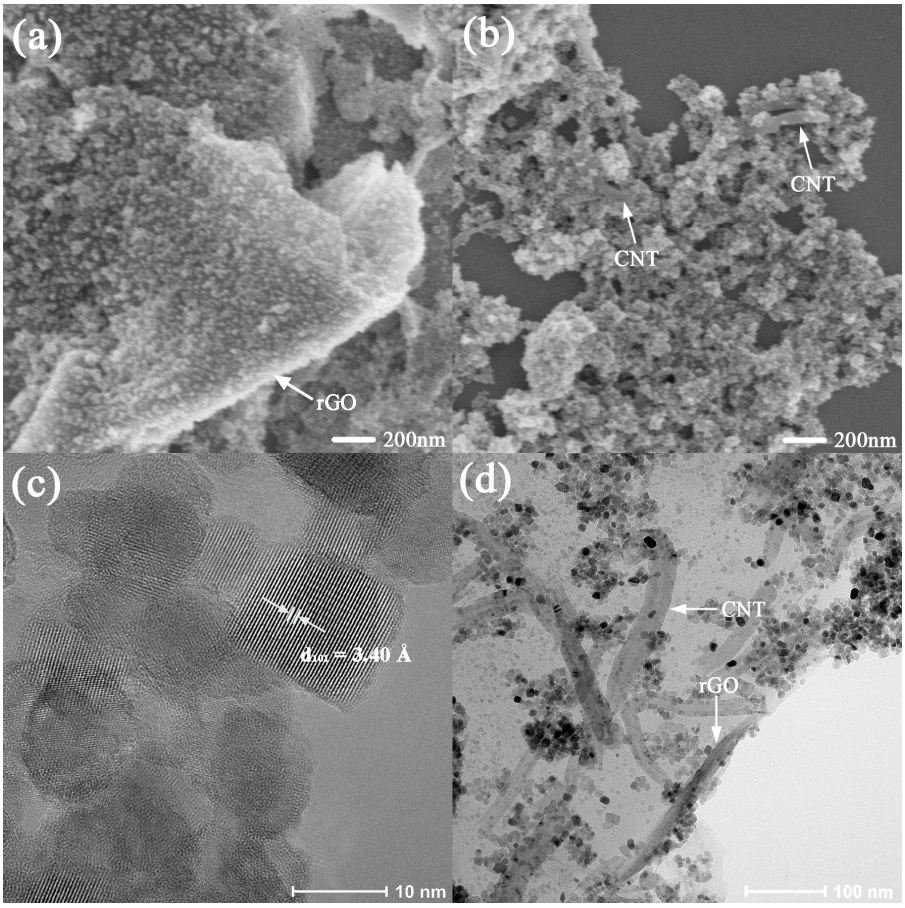

Figure 3. (**a**) Scanning electron microscopy (SEM) image of TiO_2/rGO; (**b**) SEM image of TiO_2/CNTs; (**c**) High resolution- transmission electron microscopy (HR-TEM) of TiO_2; (**d**) transmission electron microscopy (TEM) image of TiO_2/CNTs/rGO-3%.

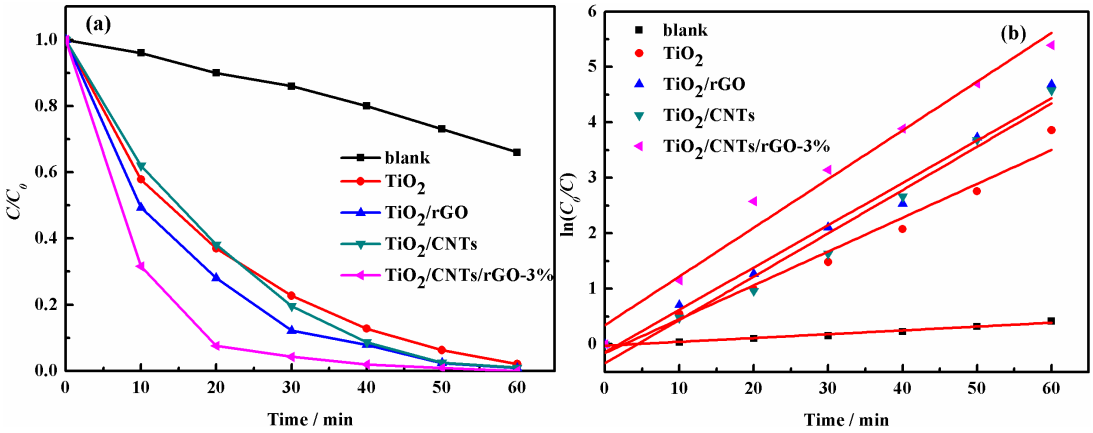

Figure 4. Blank test, TiO_2, TiO_2/rGO, TiO_2/CNTs and TiO_2/CNTs/rGO-3%: (**a**) plot of C/C_0 vs. irradiation time of RhB degradation; (**b**) linear transform $\ln(C_0/C) = kt$ of the kinetic curves of RhB degradation.

Herein, the photocatalytic degradation mechanism of TiO_2/CNTs/rGO composites was speculated. Under UV-vis irradiation, TiO_2 nanoparticles absorb light to produce photo-induced electron-hole pairs (Equation (1)) and RhB absorbs the photo flux (Equation (2)) [17]. Photo-generated electrons were seized by rGO and CNTs and transferred to the dye surface, thereby increasing the number of participating activated electrons (Equations (3) and (4)) [17]. Moreover, O_2, H_2O and organics can be adsorbed [37,38] by rGO and CNTs (Equations (5) and (6)) with a large surface area and excellent adsorption ability to further form H_2O_2 (Equation (5)) [17,39]. H_2O_2 is captured by electrons and holes promoting the formation of OH^-, OH· (Equations (7–9)) [17]. The separated holes could react with OH^- and H_2O to form OH· (Equations (10) and (11)) [6]. The activated oxidative species ($\cdot O_2{}^-$, OH·) react with the excited dye molecules which finally results in its colorless appearance. The reaction mechanism could be supposed to be

$$TiO_2 \xrightarrow{h\upsilon} TiO_2\left(h^+ + e^-\right) \quad (1)$$

$$RhB \xrightarrow{h\upsilon} RhB^*\left(h^+ + e^-\right) \quad (2)$$

$$rGO + e^- \rightarrow rGO(e^-) \quad (3)$$

$$CNTs + e^- \rightarrow CNTs(e^-) \quad (4)$$

$$rGO(e^-) + O_2 + 2H^+ \rightarrow rGO + H_2O_2 \quad (5)$$

$$H_2O_2 \xrightarrow{h\upsilon} 2OH^- \quad (6)$$

$$H_2O_2 + e^- \rightarrow OH^- + OH\cdot \quad (7)$$

$$OH^- + h^+ \rightarrow OH\cdot \quad (8)$$

$$CNTs(e^-) + O_2 \rightarrow CNTs + \cdot O_2{}^- \quad (9)$$

$$TiO_2(h^+) + OH^- \rightarrow TiO_2 + OH\cdot \quad (10)$$

$$TiO_2(h^+) + H_2O \rightarrow TiO_2 + OH\cdot \quad (11)$$

4. Conclusions

In this study, the ternary TiO_2/CNTs/rGO composites were fabricated by a facile and environmentally friendly one-pot solvethermal method. The TiO_2/CNTs/rGO-3% composites showed the most outstanding photocatalytic activity. The improved photocatalytic activity was ascribed to the synergistic effect of TiO_2, CNTs and rGO, in which TiO_2 nanoparticles absorb light to produce photo-induced electron-hole pairs, whereas rGO and CNTs can reduce electron-hole recombination, adsorb O_2, H_2O and organics from the solution and air and enhance the photocatalytic performance. This study provided new ideas regarding the carbon-based TiO_2 composites that are applied to the photocatalytic materials.

Supplementary Materials: The following are available online at http://www.mdpi.com/2079-4991/8/6/431/s1, Figure S1: The SEM images of GO, oxide-treated CNTs, CNTs/GO, TiO_2/CNTs/rGO-3%. Figure S2: The XRD patterns of rGO and GO. Figure S3: (a) The XRD patterns of TiO_2/CNTs/rGO-x% (x = 0.5, 1, 2, 3, 5, 10); (b) The Raman spectra of TiO_2/CNTs/rGO-x% (x = 0.5, 1, 2, 3, 5, 10). Figure S4: Plot of C/C_0 vs irradiation time of RhB degradation for TiO_2/CNTs/rGO-x% (x = 0.5, 1, 2, 3, 5, 10). Figure S5: The color change of RhB solution from 0, 10, 20, 30, 40, 50, 60 min under UV-vis light (from left to right).

Author Contributions: For research articles with several authors, a short paragraph specifying their individual contributions must be provided. The following statements should be used "Conceptualization, Y.H. and D.L.; Methodology, Y.H.; Software, D.C.; Validation, Y.H., Y.Q. and X.H.; Formal Analysis, Y.H.; Investigation, Y.H.; Resources, D.L.; Data Curation, D.L.; Writing-Original Draft Preparation, Y.H.; Writing-Review & Editing, D.L.; Visualization, X.H.; Supervision, D.L.; Project Administration, D.L.; Funding Acquisition, D.L.", please turn to the CRediT taxonomy for the term explanation. Authorship must be limited to those who have contributed substantially to the work reported.

Funding: This research was funded by National Nature Science Fundation of China: No. 51502098. National Nature Science Fundation of China: No. 51475175. Promotion Program for Young and Middle-aged Teacher in Science and Technology Research of Huaqiao University: ZQN-PY305. Promotion Program for Young and Middle-aged Teacher in Science and Technology Research of Huaqiao University: ZQN-YX202.

Acknowledgments: This work was supported by the National Natural Science Foundation of China (No. 51502098 and 51475175) and the Promotion Program for Young and Middle-aged Teacher in Science and Technology Research of Huaqiao University (ZQN-PY305, ZQN-YX202).

Conflicts of Interest: The authors declare no conflict of interest.

References

1. Kaneko, M.; Okura, I. *Photocatalysis: Science and Technology*; Springer: Berlin, Germany, 2002; pp. 20–25.
2. Ma, L.; Chen, A.; Zhang, Z.; Lu, J.; He, H.; Li, C. In-situ fabrication of CNT/TiO_2 interpenetrating network film on nickel substrate by chemical vapour deposition and application in photoassisted water electrolysis. *Catal. Commun.* **2012**, *21*, 27–31. [CrossRef]
3. Shah, M.S.A.S.; Zhang, K.; Park, A.R.; Kim, K.S.; Park, A.G.; Park, J.H.; Yoo, P.J. Single-stepsolvothermal synthesis of mesoporous Ag-TiO_2-reduced graphene oxide ternary composites with enhanced photocatalytic activity. *Nanoscale* **2013**, *5*, 5093–5101. [CrossRef] [PubMed]
4. Yan, W.; He, F.; Gai, S.L.; Gao, P.; Chen, Y.J.; Yang, P.P. A novel 3D structured reduced graphene oxide/TiO_2 composite: Synthesis and photocatalytic performance. *J. Mater. Chem. A* **2014**, *2*, 3605–3612. [CrossRef]
5. Gu, X.; Chai, T.; Gao, Y.H. Three dimensional TiO_2-graphene with improved adsorption capacities and photocatalytic. *Appl. Chem. Ind.* **2018**, *47*, 126–130.
6. Wang, C.; Cao, M.; Wang, P.; Ao, Y.; Hou, J.; Qian, J. Preparation of graphene-carbon nanotube-TiO_2 composites with enhanced photocatalytic activity for the removal of dye and Cr (VI). *Appl. Catal. A Gen.* **2014**, *473*, 83–89. [CrossRef]
7. Pan, X.; Zhao, Y.; Liu, S.; Korzeniewski, C.L.; Wang, S.; Fan, Z. Comparing graphene-TiO_2 nanowire and graphene-TiO_2 nanoparticle composite photocatalysts. *ACS Appl. Mater. Interfaces* **2012**, *4*, 3944–3950. [CrossRef] [PubMed]
8. Zhang, N.; Liu, S.; Fu, X.; Xu, Y.J. Synthesis of M@TiO_2 (M = Au, Pd, Pt) core-shell nanocomposites with tunable photoreactivity. *J. Phys. Chem. C* **2011**, *115*, 9136–9145. [CrossRef]
9. Xiao, F. An efficient layer-by-layer self-assembly of metal-TiO_2 nanoring/nanotube heterostructures, M/T-NRNT (M = Au, Ag, Pt), for versatile catalytic applications. *Chem. Commun.* **2012**, *48*, 6538–6540. [CrossRef] [PubMed]
10. Cao, Y.; Yang, W.; Zhang, W.; Liu, G.; Yue, P. Improved photocatalytic activity of Sn^{4+} doped TiO_2 nanoparticulate films prepared by plasma-enhanced chemical vapor deposition. *New J. Chem.* **2004**, *28*, 218–222. [CrossRef]
11. Asahi, R.; Morikawa, T.; Ohwaki, T.; Aoki, K.; Taga, Y. Visible-light photocatalysis in nitrogen-doped titanium oxides. *Science* **2001**, *293*, 269–271. [CrossRef] [PubMed]
12. Huang, Y.; Li, R.; Chen, D.; Hu, X.; Chen, P.; Chen, Z.; Li, D. Synthesis and characterization of CNT/TiO_2/ZnO composites with high photocatalytic performance. *Catalysts* **2018**, *8*, 151. [CrossRef]
13. Chen, J.S.; Luan, D.; Li, C.M.; Boey, F.Y.; Qiao, S.; Lou, X.W. TiO_2 and SnO_2@TiO_2 hollow spheres assembled from anatase TiO_2 nanosheets with enhanced lithium storage properties. *Chem. Commun.* **2010**, *46*, 8252–8254. [CrossRef] [PubMed]
14. Li, R.; Chen, D.; Huang, Y.; Hu, X.; Chen, P.; Chen, Z.; Li, D. Controllable deposition of titanium dioxides onto carbon nanotubes in aqueous solutions. *Integr. Ferroelectr.* **2016**, *183*, 43–53. [CrossRef]
15. Tu, W.; Zhou, Y.; Liu, Q.; Yan, S.; Bao, S.; Wang, X.; Xiao, M.; Zou, Z. An in situ simultaneous reduction-hydrolysis technique for fabrication of TiO_2-graphene 2D sandwich-like hybrid nanosheets: Graphene-promoted selectivity of photocatalytic-driven hydrogenation and coupling of CO_2 into methane and ethane. *Adv. Funct. Mater.* **2013**, *23*, 1743–1749. [CrossRef]
16. Shen, L.; Zhang, X.; Li, H.; Yuan, C.; Cao, G. Design and tailoring of a three-dimensional TiO_2-graphene-carbon nanotube nanocomposite for fast lithium storage. *J. Phys. Chem. Lett.* **2011**, *2*, 3096–3101. [CrossRef]
17. Rastogi, M.; Kushwaha, H.S.; Vaish, R. Highly efficient visible light mediated azo dye degradation through barium titanate decorated reduced graphene oxide sheets. *Electron. Mater. Lett.* **2016**, *12*, 281–289. [CrossRef]

18. Compton, O.C.; Nguyen, S.T. Graphene oxide, highly reduced graphene oxide, and graphene: Versatile building blocks for carbon-based materials. *Small* **2010**, *6*, 711–723. [CrossRef] [PubMed]
19. Singh, A.; Khare, P.; Verma, S.; Bhati, A.; Sonker, A.K.; Tripathi, K.M.; Sonkar, S.K. Pollutant soot for pollutant dye degradation: soluble graphene nanosheets for visible light induced photodegradation of methylene blue. *Acs Sustain. Chem. Eng.* **2017**, *5*, 8860–8869.
20. Zhang, H.; Xu, P.; Du, G.; Chen, Z.; Oh, K.; Pan, D.; Jiao, Z. A facile one-step synthesis of TiO_2/graphene composites for photodegradation of methyl orange. *Nano Res.* **2011**, *4*, 274–283. [CrossRef]
21. Shiraishi, Y.; Shiota, S.; Hirakawa, H.; Tanaka, S.; Ichikawa, S.; Hirai, T. Titanium dioxide/reduced graphene oxide hybrid photocatalysts for efficient and selective partial oxidation of cyclohexane. *ACS Catal.* **2016**, *7*, 293–300. [CrossRef]
22. Mishra, Y.K.; Adelung, R. ZnO tetrapod materials for functional applications. *Mater. Today* **2017**. [CrossRef]
23. Malekshoar, G.; Pal, K.; He, Q.; Yu, A.; Ray, A.K. Enhanced solar photocatalytic degradation of phenol with coupled graphene-based titanium dioxide and zinc oxideo. *Ind. Eng. Chem. Res.* **2014**, *53*, 18824–18832. [CrossRef]
24. Fu, S. Preparation of ZnO/TiO_2 Coupled Films and Its Photocatalytic Properties. Master's Thesis, Zhejiang University, Hangzhou, China, 2015.
25. Tyagi, A.; Tripathi, K.M.; Singh, N.; Choudhary, S.; Gupta, R.K. Green synthesis of carbon quantum dots from lemon peel waste: Applications in sensing and photocatalysis. *RSC. Adv.* **2016**, *6*, 72423–72432. [CrossRef]
26. Gogoi, S.; Karak, N. Solar-driven fydrogen peroxide production using polymer-supported carbon bots as heterogeneous catalyst. *Nano Micro. Lett.* **2017**, *9*, 40–51. [CrossRef]
27. Muhulet, A.; Miculescu, F.; Voicu, S.; Fabian Schütt, F.; Thakur, V.K.; Mishra, Y.K. Fundamentals and scopes of doped carbon nanotubes towards energy and biosensing applications. *Mater. Today Energy* **2018**, *9*, 154–186. [CrossRef]
28. Xiong, H.; Motchelaho, M.A.; Moyo, M.; Jewell, L.L.; Coville, N.J. Fischere-tropsch synthesis: Iron-based catalysts supported on nitrogen-doped carbon nanotubes synthesized by post-doping. *Appl. Catal. A Gen.* **2014**, *482*, 377–386. [CrossRef]
29. Jiang, S.; Handberg, E.S.; Liu, F.; Liao, Y.; Wang, H.; Li, Z.; Song, S. Effect of doping the nitrogen into carbon nanotubes on the activity of NiO catalysts for the oxidation removal of toluene. *Appl. Catal. B Environ.* **2014**, *160*, 716–721. [CrossRef]
30. Zhang, Q.; Fan, W.; Gao, L. Anatase TiO_2, nanoparticles immobilized on ZnO tetrapods as a highly efficient and easily recyclable photocatalyst. *Appl. Catal. B Environ.* **2007**, *76*, 168–173. [CrossRef]
31. Liu, B.; Zeng, H.C. Carbon nanotubes supported mesoporous mesocrystals of anatase TiO_2. *Chem. Mater.* **2008**, *20*, 2711–2718. [CrossRef]
32. Tetty, K.E.; Yee, M.Q.; Lee, D. Photocatalytic and conductive MWCNT/TiO_2 nanocomposite thin films. *ACS Appl. Mater. Interfaces* **2010**, *2*, 2646–2652. [CrossRef] [PubMed]
33. Yen, C.Y.; Lin, Y.F.; Hung, C.H.; Tseng, Y.H.; Ma, C.C.; Chang, M.C.; Shao, H. The effects of synthesis procedures on the morphology and photocatalytic activity of multi-walled carbon nanotubes/TiO_2 nanocomposites. *Nanotechnology* **2008**, *19*, 045604–045614. [CrossRef] [PubMed]
34. Zhang, M.; Wang, Y.; Pan, D.; Li, Y.; Yan, Z.; Xie, J. Nitrogen-doped 3D graphene/MWNTs nano-frameworks embedded Co_3O_4 for high electrochemical performance supercapacitors. *ACS Sustain. Chem. Eng.* **2017**, *5*, 5099–5107. [CrossRef]
35. Wang, C.; Xu, J.; Yuen, M.; Zhang, J.; Li, Y.; Chen, X.; Zhang, W. Hierarchical composite electrodes of nickel oxide nanoflake 3D graphene for high-performance pseudocapacitors. *Adv. Funct. Mater.* **2015**, *24*, 6372–6380. [CrossRef]
36. Fan, Z.; Yan, J.; Zhi, L.; Zhang, Q.; Wei, T.; Feng, J.; Zhang, M.; Qian, W.; Wei, F. A three-dimensional carbon nanotube/graphene sandwich and its application as electrode in supercapacitors. *Adv. Mater.* **2010**, *22*, 3723–3728. [CrossRef] [PubMed]
37. Min, S.; Lu, G. Advance in Photocatalyst Based on Graphene. In *Analysis and Testing Technology and Instruments*; CNKI: Beijing, China, 2014; pp. 215–229.
38. Zhou, B. First-Principles Study of Chemisorption and Diffusion of Small Molecules on Carbon Nanotubes. Doctoral Thesis, Nanjing University of Aeronautics and Astronautics, Nanjing, China, 2008.

39. Sampaio, M.J.; Benyounes, A.; Serp, P.; Faria, J.L.; Silva, C.G. Photocatalytic synthesis of vanillin using N-doped carbon nanotubes/ZnO catalysts under UV-LED irradiation. *Appl. Catal. A Gen.* **2017**, *551*, 71–78. [CrossRef]
40. Lv, R.; Cruzsilva, E.; Terrones, M. Building complex hybrid carbon architectures by covalent interconnections: Graphene-nanotube hybrids and more. *ACS Nano* **2014**, *8*, 4061–4069. [CrossRef] [PubMed]

© 2018 by the authors. Licensee MDPI, Basel, Switzerland. This article is an open access article distributed under the terms and conditions of the Creative Commons Attribution (CC BY) license (http://creativecommons.org/licenses/by/4.0/).